

Absolute differential cross sections for small-angle H^+ -He direct and charge-transfer scattering at keV energies

L. K. Johnson, R. S. Gao, R. G. Dixson, K. A. Smith, N. F. Lane, and R. F. Stebbings
*Department of Physics, Department of Space Physics and Astronomy, and Rice Quantum Institute,
Rice University, P.O. Box 1892, Houston, Texas 77251*

M. Kimura

*Department of Physics, Rice University, Houston, Texas 77251
and Argonne National Laboratory, ER 203, 9700 Cass Avenue, Argonne, Illinois 60439*

(Received 27 March 1989; revised manuscript received 21 June 1989)

This paper reports measurements and calculations of absolute differential cross sections for H^+ -He charge-transfer and direct scattering. Charge-transfer measurements have been obtained at 5.0 keV laboratory energy over the laboratory angular range 0.02° – 1.0° , while direct scattering has been observed at 0.5, 1.5, and 5.0 keV laboratory energy over a closely corresponding angular range. Calculations are reported for 0.5, 1.5, and 5.0 keV charge-transfer and direct scattering. The measured cross sections are in good agreement with those derived from fully quantum-mechanical molecular-orbital close-coupling calculations. Direct scattering cross sections are also found to be in agreement with single-potential calculations using directly summed Jeffreys-Wentzel-Kramers-Brillouin phase shifts derived from proposed H^+ -He ground-state interaction potentials. The cross sections exhibit significant structure over the range of angles and energies studied. The measured cross sections have been integrated over the experimental angular range providing absolute integral cross sections for comparison with theoretical results and previously measured total cross sections.

I. INTRODUCTION

Studies of angular differential scattering at keV energies in ion-atom collisions at very small angles (below 1°) are motivated by the highly forward-peaked character of the cross sections and by the location of the classical rainbow angle within this range. This paper reports measurements of absolute differential cross sections for direct and charge-transfer scattering of keV energy protons from neutral helium. The high angular resolution of the apparatus allows detailed observations of structure in the vicinity of the classical rainbow maximum.

Oscillatory patterns seen in elastic and inelastic scattering have been studied extensively using semiclassical scattering theories. In particular, the models of Landau, Zener, and Stueckelberg¹ (LZS) for potential curve crossings and of Demkov² for pseudocrossings have been used successfully to describe characteristics of quantum interference in some heavy-particle collisions where primarily two states are involved. In these models, it is assumed that a transition between the initial and final state takes place in a well-localized region as the two particles are approaching or receding from each other. Interference between the scattering amplitudes for these two cases is responsible for oscillatory structure in the cross sections. In the present work, a theoretical study has been undertaken to investigate such interference phenomena without resorting to approximations such as the Demkov or LZS models. Theoretical cross sections, differential in angle, for direct and charge-transfer

scattering have been obtained for the H^+ -He system from a fully quantum-mechanical, close-coupling calculation based on molecular-orbital (MO) techniques. A single-potential Jeffreys-Wentzel-Kramers-Brillouin (JWKB) partial-wave analysis using H^+ -He ground-state potentials discussed by Helbig *et al.*³ has also been performed to obtain direct scattering cross sections.

Comparisons between theory and experiment permit evaluation of the theoretical interaction potentials at internuclear distances of a few angstroms. In addition, experimental differential cross sections are integrated over angle to provide absolute integral cross sections for comparison with the results of the MO theory and with previously measured total cross sections.

II. APPARATUS AND EXPERIMENTAL METHOD

Figure 1 shows a schematic of the apparatus, which has been previously described in detail.^{4,5} Protons emerging from the electron-impact ion source are accelerated to the desired energy and focused by an electrostatic lens. The resulting beam is momentum analyzed by a pair of 60° sector magnets and passes through a collimating aperture before arriving at the target cell (TC). A positive-sensitive detector (PSD) is located on axis downstream to monitor both the primary ion beam and the fast neutral collision products. Deflection plates (DP) may be used to prevent ions from striking the detector. The collimating aperture and the entrance aperture of the TC are 20 and 30 μm in diameter, respectively, and are

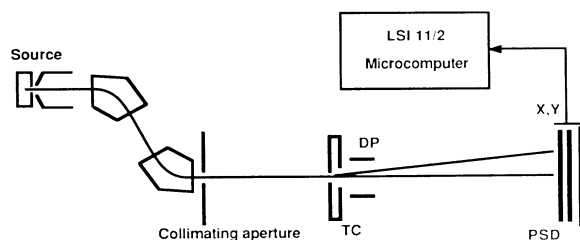


FIG. 1. Schematic of the apparatus.

separated by 49 cm, thereby collimating the ion beam to less than 0.003° divergence. The TC has a length of 0.38 cm and an exit aperture $300\ \mu\text{m}$ in diameter. A PSD with an active area 4.0 cm in diameter is axially located 109 cm beyond the TC, permitting a maximum observable scattering angle of about 1.3° . An LSI 11/2 microcomputer monitors the output of the PSD electronics, sorting the arrival coordinates of each detected particle into bins in a 90×90 array. The physical area corresponding to the bin size is variable, so that the conflicting requirements of high resolution and large angular coverage may be met. The minimum physical bin size for the present experiments is $109 \times 109\ \mu\text{m}^2$. The bin size is measured by observing the shadow of a nickel grid of known dimensions placed directly in front of the detector as an ion beam is swept over the detector surface. This technique is also used to determine the position-finding accuracy of the PSD. For the charge-transfer experiment, the primary ion-beam flux is measured intermittently during the neutral particle accumulation by removing the electric field established between the DP. The issue of possibly differing detection efficiencies for neutral and charged species has been discussed previously^{5,6} with the conclusion that the two efficiencies are considered equal at 5.0 keV.

Under the thin-target conditions used in this experiment, the differential cross section is determined from the measured quantities by the expression

$$\frac{d\sigma(\theta)}{d\Omega} = \frac{\Delta S(\theta)}{S\tau\Delta\Omega}, \quad (1)$$

where S is the primary ion-beam flux in particles per second, $\Delta S(\theta)$ is the neutral flux scattered at angle θ into a solid angle $\Delta\Omega$ steradians, and τ is the target thickness. For the present geometry, τ has previously⁴ been determined to be accurately given by the product nL , where n is the number density obtained from a measurement of gas pressure in the TC and L is the physical length of the cell. At a typical target cell pressure of 5 mtorr, residual vacuum chamber pressure is maintained below 2×10^{-7} torr. Under these conditions, only 5% of the beam is scattered by the target gas, making multiple collision effects negligible.

A description of the data acquisition and analysis technique has been presented by Nitz *et al.*⁴ and only a brief discussion will be provided here. For charge-transfer and direct scattering, two 90×90 data files, one with gas in the target cell and one without, are taken. The scattered

flux, $\Delta S(\theta)$, is obtained by organizing the 90×90 data arrays into concentric rings and subtracting the gas-out data from the gas-in data. This procedure permits discrimination between counts due to scattering from the target gas and counts arising from other sources, such as PSD dark counts or scattering from the background gas or from edges of apertures. For direct scattering, additional files must be accumulated to properly account for counts on the detector due to neutral collision products.

The experimental uncertainty in the number of counts at a particular angle is primarily statistical, and ranges from 1% near 0.05° to 10% near 1° . The angular uncertainty arises from the finite width of the primary ion beam, the discrete width of the analysis rings, and electronic errors in the detector's position encoding circuits, and amounts to about 0.02° at the smallest scattering angles. The effect of the finite angular resolution of the apparatus has been estimated by Gao *et al.*,⁵ who calculated the convolution of He^+ -He theoretical cross sections with an apparatus function which accounts for the above-mentioned effects. Their calculation raised the minima in the strongly oscillating He^+ -He cross section only at very small angles ($\sim 0.05^\circ$). Convolution of the present direct scattering calculations would not change the cross sections appreciably, since their structure is less pronounced.

III. THEORETICAL CONSIDERATIONS

Previous molecular-orbital (MO) studies⁷ have revealed that in H^+ -He collisions below 20 keV, charge transfer to the $\text{H}(1s)$ state dominates all other charge-transfer and excitation processes, having more than an order of magnitude larger cross section than both $\text{H}(2p)$ transfer and ionization. As the energy is increased above 60 keV, ionization becomes the most significant process. Thus a two-state MO close-coupling calculation should provide satisfactory cross sections for the dominant channels in the energy range studied, i.e., $E \leq 5$ keV.

In a fully quantum-mechanical formulation of heavy-particle collisions at low energy,⁸ the total time-independent scattering wave function of the system is described in an adiabatic representation as an expansion in products of electronic (Born-Oppenheimer) and nuclear wave functions

$$\Psi(\mathbf{R}, \mathbf{r}) = \sum_i F_i(\mathbf{R}, \mathbf{r}) \chi_i^a(\mathbf{R}), \quad (2)$$

where $F_i(\mathbf{R}, \mathbf{r})$ represents the Born-Oppenheimer electronic wave function for fixed internuclear coordinates \mathbf{R} and all electronic coordinates \mathbf{r} , including electron-translation factors (ETF's); the $\chi_i^a(\mathbf{R})$ represents the nuclear (scattering) wave functions that correspond to the electronic states i in the adiabatic representation. Substitution of this equation into the stationary Schrödinger equation yields coupled, second-order differential equations for the $\chi_i^a(\mathbf{R})$. It is computationally convenient to solve these equations in a diabatic representation. The unitary transformation matrix $\mathbf{C}(\mathbf{R})$, satisfying $\chi^a(\mathbf{R}) = \mathbf{C}(\mathbf{R})\chi^d(\mathbf{R})$, where $\chi^{a,d}(\mathbf{R})$ are column vectors, is introduced to transform to the diabatic representation, in which the radial derivative coupling terms are zero. The

resulting coupled equations are in matrix form,

$$\left[\frac{1}{2\mu} \nabla_{\mathbf{R}}^2 \mathbf{I} - \mathbf{V}^d(\mathbf{R}) + E \mathbf{I} \right] \chi^d(\mathbf{R}) = 0, \quad (3)$$

where μ is the reduced mass of the system, \mathbf{I} is the identity matrix, and \mathbf{V}^d , the diabatic potential matrix, is related to its adiabatic counterpart by $\mathbf{V}^d = \mathbf{C}^{-1} \mathbf{V}^a \mathbf{C}$. Since only two states are considered in the present work, Eq. (3) consists of two coupled scalar equations, which are solved to obtain the scattering S matrix for each partial wave (for the spherically symmetric case) using the log-derivative method.⁹ The differential cross section for charge transfer is then obtained from the formula

$$\frac{d\sigma(\Theta)}{d\Omega} = \frac{1}{4k^2} \left[\sum_l (2l+1) S_{12}^l P_l(\cos\Theta) \right]^2, \quad (4)$$

where S_{12}^l is the scattering S -matrix element for partial wave l , Θ is the scattering angle in center-of-mass coordinates, and k is the momentum of the projectile. A similar equation with $(1 - S_{11}^l)$ in place of S_{12}^l is used to obtain the direct elastic-scattering cross sections. The number of partial waves needed to obtain reasonable convergence of cross sections is 1800 for 1.5 keV and 3200 for 5.0 keV (laboratory frame energies). Full configuration-interaction calculations were performed to obtain eigenvalues and eigenfunctions of the electronic Hamiltonian. Slater-type orbitals (STO) were employed as basis functions. Values of the orbital exponents for the STO's are found in Ref. 7. The calculated adiabatic potential curves for the initial $\text{H}^+ - \text{He}(1^1S)$ and final $\text{H}(1s) - \text{He}^+(1s)$ states are plotted in Fig. 2, along with the nonadiabatic radial coupling matrix element (where the opti-

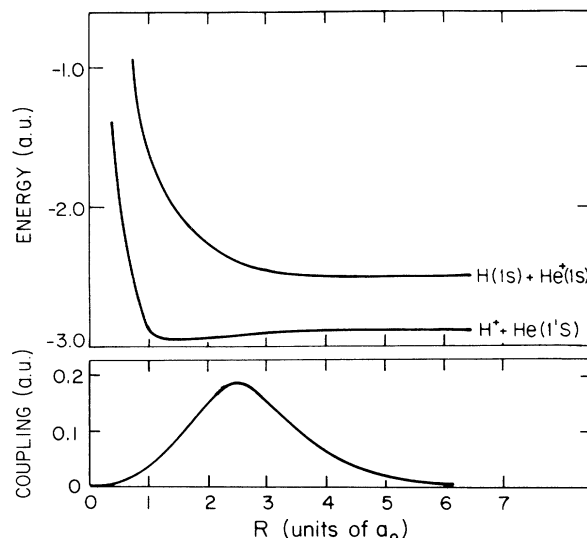


FIG. 2. Adiabatic potentials and corresponding radial coupling between the two states, calculated from the MO theory.

mized MO-ETF has been used⁷) between these states. Representative values of the potentials have been tabulated in Table I as an aid to other investigators.

Direct scattering cross sections have also been calculated through the use of single-channel potential scattering models, closely following Nitz *et al.*⁴ Theoretical interaction potentials from other investigations are used in a partial-wave analysis with semiclassical phase shifts. This approach is satisfactory because the small-angle

TABLE I. Calculated values for the adiabatic radial coupling, initial-state, and final-state potential-energy curves, using the MO theory. Internuclear distance is given in a_0 , while energies are stated in a.u.

Internuclear r (units of a_0)	Coupling	Potential energy (a.u.)	
		$\text{H}^+ - \text{He}(1s^2)$	$\text{H}(1s) - \text{He}^+(1s)$
0.10		12.87	15.05
0.20		3.156	5.246
0.30	0.0	0.1395	2.121
0.40	0.002	-1.219	0.6579
0.50	0.006	-1.934	-0.1652
0.60	0.010	-2.344	-0.6812
0.70	0.016	-2.590	-1.027
0.80	0.021	-2.742	-1.273
0.90	0.029	-2.836	-1.457
1.00	0.036	-2.895	-1.599
1.50	0.089	-2.967	-2.028
2.00	0.150	-2.947	-2.256
2.50	0.185	-2.926	-2.382
3.00	0.150	-2.913	-2.446
3.50	0.100	-2.907	-2.477
4.00	0.060	-2.903	-2.490
4.50	0.035	-2.902	-2.496
5.00	0.021	-2.902	-2.497
6.00	0.008	-2.902	-2.498
7.50	0.002	-2.902	-2.499
10.0	0.0	-2.902	-2.499

scattering reported in this paper arises from very small deflections of the projectile at relatively large impact parameters. Two different approximations, the Jeffreys-Wentzel-Kramers-Brillouin (JWKB) and the Jeffreys-Born (JB), have been used for the phase shifts, typically several thousand partial waves are used, and the phase shifts are directly summed over l using the Rayleigh-Faxen-Holtzmark equation. The potentials used are those found in Helbig *et al.*,³ which are analytical fits to the theoretical results of Michels¹⁰ and Wolniewicz.¹¹

IV. RESULTS AND DISCUSSION

Measured and calculated cross sections are shown in Figs. 3–5 along with the 5.0-keV experimental results of Fitzwilson and Thomas,¹² which are in good agreement with the experimental data. Charge-transfer cross sections could not be experimentally obtained at energies lower than 5.0 keV since the total cross section rapidly decreases with decreasing energy. Direct scattering results are shown together with the results of the present two-state MO close-coupling theory and with the results of the JWKB calculation from the potential of Wolniewicz. The result from the potential of Michels lies very close to that of Wolniewicz, which is not surprising since these two potentials differ primarily in well depth, and there only by about 0.2 eV. Charge-transfer experimental results are shown together with calculated cross sections from the present MO theory. The structure in the cross sections may be interpreted as a consequence of several effects. Classical one-potential, trajectory-dependent effects (such as rainbow scattering from the attractive part of the H^+ -He ground-state potential) are responsible for some structure in the data. The classical rainbow maxima have been determined by calculating the deflection function, and are located at $\theta = 0.32^\circ$ (0.5 keV), 0.11° (1.5 keV), and 0.03° (5.0 keV). Gentle undulations occur in the cross sections due to quantum diffraction¹³ (arising in scattering from any steeply rising repulsive po-

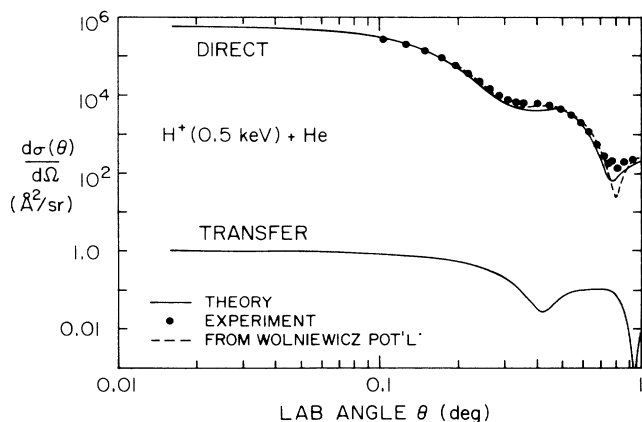


FIG. 3. Experimental data for $H^+(0.5 \text{ keV})$ -He direct scattering and theoretical predictions for differential cross sections of $H^+(0.5 \text{ keV})$ -He direct and charge-transfer scattering.

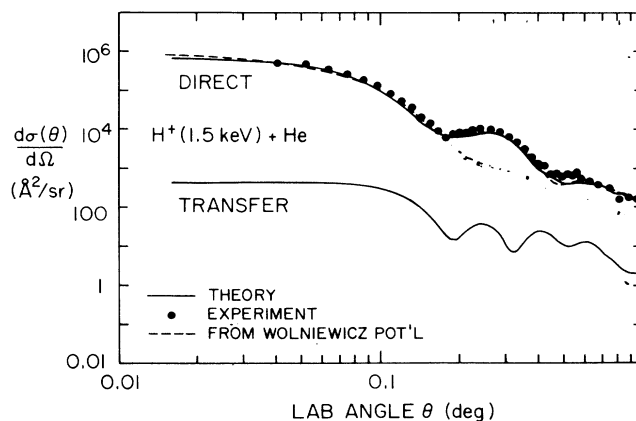


FIG. 4. Experimental data for $H^+(1.5 \text{ keV})$ -He direct scattering and theoretical predictions for differential cross sections of $H^+(1.5 \text{ keV})$ -He direct and charge-transfer scattering.

tential wall). Interference due to coupling between the direct and charge-transfer channels is responsible for “Demkov oscillations” in the cross sections. In the Demkov model,² a pseudocrossing radius R_x is defined as the separation where the nonadiabatic coupling reaches a maximum, in the present case about $2.5a_0$ (1.3 Å), as seen in Fig. 2. If the classical turning point is less than R_x , the charge-transfer channel becomes important, as shown by the S -matrix elements illustrated in Fig. 6 for a scattering energy of 1.5 keV. (The values of the impact parameters that correspond semiclassically to the respective partial-wave angular momenta are also shown.)

As an aid to interpretation of the quantum-mechanical results, it is instructive to consider the semiclassical charge-transfer deflection function, which was calculated some time ago for the single energy 1.5 keV. The deflection function, shown in Fig. 7, exhibits a branch at $l_x = 820$ or $b_x = 2a_0$ (1.1 Å). Thus for angles greater than

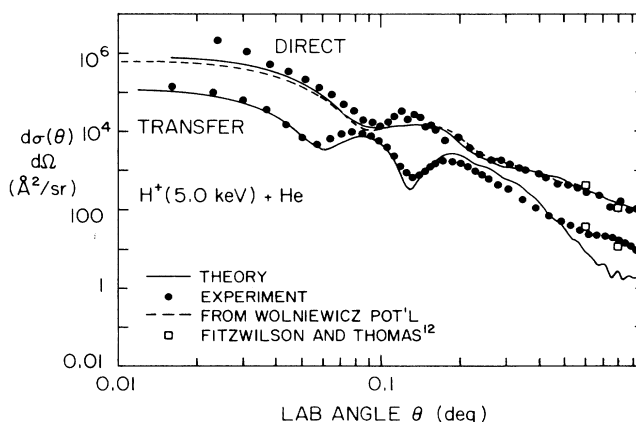


FIG. 5. Experimental data and theoretical predictions for differential cross sections of $H^+(5.0 \text{ keV})$ -He direct and charge-transfer scattering.

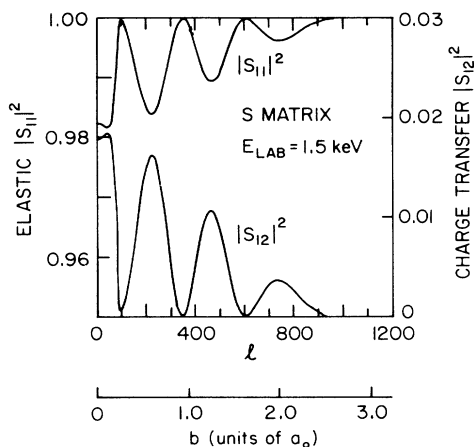


FIG. 6. Absolute value of the S -matrix element, derived from the MO theory, for direct as well as charge-transfer processes, as a function of partial-wave l (upper abscissa) and impact-parameter b (lower abscissa).

$\theta = \theta(l_x)$, structure in the cross section arises from interference between semiclassical scattering amplitudes corresponding to two different trajectories. In Fig. 7 one notes a range of impact parameters, $1.5 < b < 2.0a_0$, for which the scattering takes place around $E\theta \approx 0.18$ keV deg. This (lower) branch corresponds to a trajectory in which the particles follow the initial-channel potential inward to the classical turning point and then switch to the final-channel potential in the vicinity of $R = R_x$ on the outward portion of the trajectory. The upper branch of the deflection function corresponds to a trajectory in which the particles switch to the final-channel potential on the initial approach and then remain on this potential throughout the collision. The long-range repulsive wall of the final-channel potential gives rise to the larger deflection angles. Since each trajectory possesses a scattering amplitude with a characteristic phase, it follows that for all scattering angles $\theta > \theta_x$, interference effects will give rise to oscillatory structure in the cross

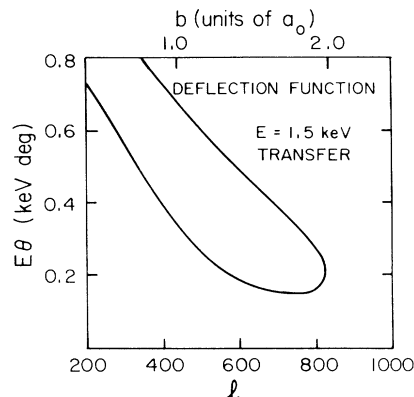


FIG. 7. Semiclassical deflection function [in the center-of-mass (c.m.) frame] for 1.5-keV charge-transfer scattering, calculated from the adiabatic potentials, as a function of partial-wave l (lower abscissa) and impact-parameter b (upper abscissa).

sections, which can be written in the simple form

$$\frac{d\sigma(\theta)}{d\Omega} \propto A - B \cos[\eta_1(b_1) - \eta_2(b_2)], \quad (5)$$

where $kb \approx l$, A and B are weak functions of impact parameter and energy, and $\eta_1(b_1), \eta_2(b_2)$ are semiclassical phase shifts at given impact parameters b_1, b_2 for trajectories denoted by 1 and 2. Variations in the difference between phase shifts ($\eta_1 - \eta_2$) as a function of angle θ (or b) lead to the oscillatory structure apparent in the experimental data. This interference is seen in the 5.0-keV charge-transfer results (see Fig. 5) for $0.04^\circ \leq \theta \leq 0.3^\circ$ and in the 1.5-keV results (see Fig. 4) at larger angles. It should also be noted that oscillations for direct and charge-transfer scattering are out of phase, as can be expected from considerations of flux loss and gain between coupled channels.

The experimental and theoretical results generally

TABLE II. Absolute integral cross sections in \AA^2 . Differential cross sections from the experiment have been integrated over the experimental angular range; those from the MO theory have been integrated over the experimental angular range (Int.) and over all angles (Tot.). The letter D denotes direct scattering while CT denotes charge-transfer scattering. Comparisons to the literature have been made where available.

Process	θ range	Expt.	Theor.		Literature
			Int.	Tot.	
$H^+(0.5 \text{ keV})\text{-He}, D$	$0.08^\circ\text{--}1.2^\circ$	7.2	7.1	10.7	
$H^+(1.5 \text{ keV})\text{-He}, D$	$0.040^\circ\text{--}0.882^\circ$	4.0	3.4	4.7	
$H^+(5.0 \text{ keV})\text{-He}, D$	$0.02^\circ\text{--}1.0^\circ$	2.3	1.6	2.2	
$H^+(0.5 \text{ keV})\text{-He}, CT$	$0^\circ\text{--}1.0^\circ$		9.9×10^{-5}	3.4×10^{-4}	
$H^+(1.5 \text{ keV})\text{-He}, CT$	$0^\circ\text{--}1.0^\circ$		0.014	0.022	0.02 ^a
$H^+(5.0 \text{ keV})\text{-He}, CT$	$0^\circ\text{--}1.2^\circ$	0.29	0.30	0.30	0.30 ^a , 0.35 ^b , 0.37 ^c

^aStedeford and Hasted (Ref. 14).

^bStier and Barnett (Ref. 15).

^cBecker and Scharmann (Ref. 16).

agree well. The direct scattering cross sections correspond very closely to both the theoretical MO predictions and to the single-potential calculations from the *ab initio* Wolniewicz and Michels potentials. The ground-state potential obtained from the MO theory lies very close to the results of the large *ab initio* calculations, with a well-depth value between those of Michels and Wolniewicz. The MO theory charge-transfer cross sections exhibit a lesser degree of agreement with experiment. Since the ground-state potential is well established by the direct scattering results, the deviations may be due to either the coupling or the H-He⁺ state potential. Preliminary calculations using the present formalism of charge-transfer theory for other rare-gas-hydride systems indicate that the angular positions of oscillation minima in charge-transfer differential cross sections are sensitive to small adjustments in the internuclear separation of the peak of the nonadiabatic coupling.

The measured differential cross sections have also been integrated over the observed angular range and compared

in Table II to total charge-transfer cross sections measured by Stedeford and Hasted,¹⁴ Stier and Barnett,¹⁵ and Becker and Scharmann.¹⁶ Such comparisons are possible because the differential cross sections are strongly peaked in the forward direction, and so the bulk of the total cross-section results from scattering inside the range of the measurements. Table II also shows total and integrated cross sections calculated from the present MO theory; the integrated experimental cross sections are in reasonable agreement with the MO results.

ACKNOWLEDGMENTS

This work was supported by the Robert A. Welch Foundation, NASA, and the National Science Foundation (NSF) Atmospheric Sciences Section, and the U.S. Department of Energy (D.O.E.), Offices of Health and Environmental Research (M.K.) and of Basic Energy Sciences, Division of Chemical Sciences (N.F.L. and R.G.D.).

¹L. D. Landau, Z. Phys. Sov. Union **2**, 46 (1932); C. Zener, Proc. R. Soc. London, Ser. A **137**, 696 (1932); E. C. G. Stueckelberg, Helv. Phys. Acta **5**, 370 (1932).

²Y. N. Demkov, Zh. Eksp. Teor. Fiz. **45**, 195 (1963) [Sov. Phys.—JETP **18**, 138 (1964)].

³H. F. Helbig, D. B. Millis, and L. W. Todd, Phys. Rev. A **2**, 771 (1970).

⁴D. E. Nitz, R. S. Gao, L. K. Johnson, K. A. Smith, and R. F. Stebbings, Phys. Rev. A **35**, 4541 (1987).

⁵R. S. Gao, L. K. Johnson, J. H. Newman, K. A. Smith, and R. F. Stebbings, Phys. Rev. A **38**, 2789 (1988).

⁶R. S. Gao, P. S. Gibner, J. H. Newman, K. A. Smith, and R. F. Stebbings, Rev. Sci. Instrum. **55**, 1756 (1984).

⁷M. Kimura, Phys. Rev. A **31**, 2158 (1985); see also the AO-MO

matching results in M. Kimura and C. D. Lin, Phys. Rev. A **34**, 176 (1986).

⁸F. T. Smith, Phys. Rev. **179**, 111 (1969).

⁹B. R. Johnson, J. Comput. Phys. **13**, 445 (1973).

¹⁰H. H. Michels, J. Chem. Phys. **44**, 3834 (1966).

¹¹L. Wolniewicz, J. Chem. Phys. **43**, 1087 (1965).

¹²R. L. Fitzwilson and E. W. Thomas, Phys. Rev. A **6**, 1054 (1972).

¹³H. J. Beier, J. Phys. B **6**, 683 (1973).

¹⁴J. B. H. Stedeford and J. B. Hasted, Proc. R. Soc. London, Ser. A **227**, 466 (1955).

¹⁵P. M. Stier and C. F. Barnett, Phys. Rev. **103**, 896 (1956).

¹⁶M. Becker and A. Scharmann, Z. Naturforsch. **24**, 854 (1969).